



Theoretical and numerical investigations on mining-induced fault activation and groundwater outburst of coal seam floor

Wencheng Song^{1,2} · Zhengzhao Liang^{1,2}

Received: 27 April 2020 / Accepted: 12 April 2021 / Published online: 5 May 2021
© Springer-Verlag GmbH Germany, part of Springer Nature 2021

Abstract

Mining activities carried out above an aquifer, especially in the hanging wall of normal faults, generally involve the risk of water inrush. For a better understanding of the mechanism inducing groundwater outburst through fault floor, the analytical and numerical simulation methods were applied to investigate the process of fault activation driven by mining and hydraulic loads. The influences of the advancing distance and fault dip were conducted. The results exhibit good agreement between the theoretical calculation and the numerical simulation. The fault activation by induced tangential stress change has a positive correlation with the advancing distance and a negative correlation with the fault dip angle. The stress concentration factor increases significantly when the excavation process enters the horizontal range of fault projection, following the stress peak and failure zone approaching the coal seam from deep to shallow along the fault. For the cases with a constant advancing distance, the smaller the fault dip is, the earlier the water-inrush channel will be formed. The research results in this study reveal the theoretical mechanism of fault activation and groundwater inrush of coal seam floor above a confined aquifer and thus provide valuable insights for the prevention and risk assessment of mine water disasters in underground engineering.

Keywords Mining engineering · Fault activation · Tangential stress · Analytical model · Numerical simulation

Introduction

Generally, the strata containing geological structures (i.e., fault zones) show a weaker strength and are prone to mining accidents (Donnelly 2006; Islam and Shinjo 2009; Wu et al. 2004, 2020). When human activities are carried out above the aquifer, the redistribution of ground stress field may lead to fault activation (Liu et al. 2018; Sainoki and Mitri 2018) and potentially further improve the permeability of fault zone, thus forming a highly permeable channel for groundwater outburst. This has resulted in both significant casualties and intermittent production to the underground coal mines (Bukowski 2011; Lamoreaux et al. 2014; Xue et al. 2021). As shown in Fig. 1,

the formation of water gushing channels in the seam floor strata is mainly involved with intrinsic faults (Lu and Wang 2015; Shao et al. 2019), karst collapse pillars (KCPs) (Li and Zhou 2006), and randomly distributed fractures (Liang et al. 2019; Wu et al. 2019). Moreover, the existence of fault zone, as the major geological discontinuity, directly weakens the water-resisting capacity of key strata between coal body and correlative aquifer. Statistics reveal that more than 80% of inrush catastrophes encountered in engineering have an impartible relationship with the geological fault (Bai et al. 2013; Shi et al. 2018; Zhang et al. 2014). Therefore, understanding the activation mechanism of faults has practical significance for the prevention and control of mine water disasters.

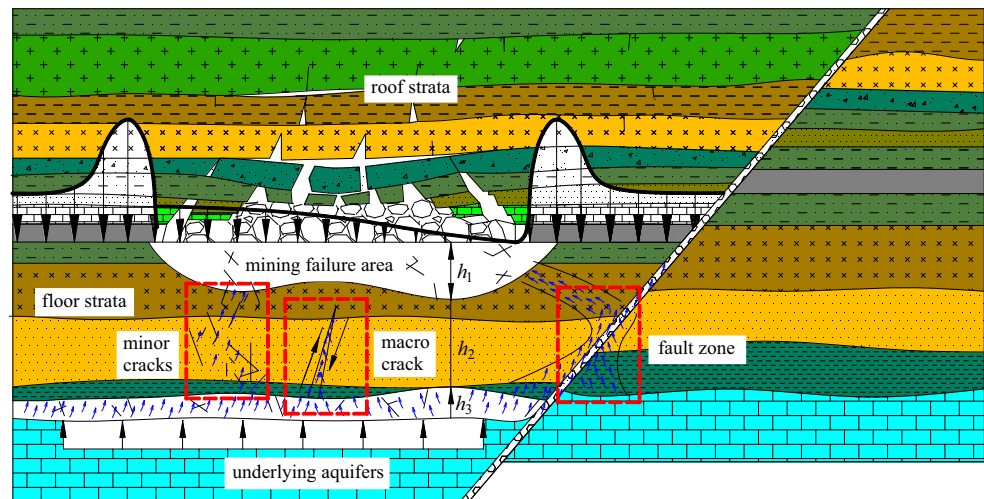
For decades, the contributing mechanism of fault-activated inrush hazards in underground mines has been widely concerned by many scholars and operators. For example, Bu and Xu (2020) and Hu et al. (2014) calculated the distribution of stress filed on the fault plane by using simplified mechanical models and further explained the mechanism of fault re-activation induced by mining. Sun et al. (2019) and Hu et al. (2019) proposed analytical models based on the hypothesis of limit equilibrium and successfully predicted the critical water-proof capacity of fault floor after coal excavation. Liu et al.

✉ Zhengzhao Liang
LiangZZ@dlut.edu.cn

¹ State Key Laboratory of Coastal and Offshore Engineering, Dalian University of Technology, Dalian 116024, Liaoning, China

² Center of Rock Instability and Seismicity Research, Dalian University of Technology, Dalian 116024, Liaoning, China

Fig. 1 Types of water inrush from the underlying aquifers. h_1 , the depth of mining failure zone; h_2 , the thickness of remaining water-proof zone; h_3 , the height of hydraulic ascending zone



(2020) theoretically studied the influential laws of the advancing distance on water inrush associated with faults. These issues have also been highlighted with respect to numerical modeling, physical simulation, and field measurement. Li et al. (2011) numerically simulated the evolution of damage and seepage characteristics along faults during the mining process. Yang et al. (2017) analyzed the correlation between macroscopic permeability and the scale of jointed rock mass using an improved coupling model. According to the laboratory results of Zhu et al. (2018) and Zhang et al. (2017), the direct cause inducing groundwater outburst was the complete hydraulic connection of fractured zones between the fault and the “intact” floor. Cheng et al. (2019) analyzed the effect fault parameters on micro-seismic monitoring events and divided the fault activities into five stages. Other useful analytical models and methods have also been put forward successively (Huang et al. 2014; Li et al. 2019; Shi et al. 2019; Xu et al. 2012; Zhu and Wei 2011). These investigations are of great importance to improve the safety of coal extraction above the confined aquifer. However, the essence of water inrush from coal seam floor is the result of combined action of mining and hydraulic pressures (Gudmundsson et al. 2001; Yin et al. 2015). The above theoretical models do not consider the effect of confined water, which also plays a vital role in promoting the re-activation of the fault.

Consequently, a mechanical model of fault floor driven by mining and hydraulic loads was proposed to analyze the process of fault activation. Moreover, the pathways for groundwater outburst from the underlying aquifer after coal excavation were numerically investigated using Fast Lagrangian Analysis of Continua (FLAC3D). The comparative results of this study could provide some valuable insights for fault water inrush of underground engineering.

Engineering geology

As shown in Fig. 2, Huatai Coal Mine is located about 5.5 km southeast of Laiwu City, Shandong Province, China, covering a field area of approximately 27.3 km². There are Nos. 2, 4, 7, and 15 coal seams that are available for mining. Among them, No. 7 coal seam is near-horizontal seam with an average thickness of 4 m and a buried depth of 650 m. The excavation dimensions of the No. 7502 working face along the strike and inclination are 800 m and 150 m respectively, and the total caving method is adopted for roof management. The normal fault F_{qin} , which affects the excavation process of the working face, belongs to the main structure in the middle of the coalfield, with a dip angle of 35–65° (average 45°), a fault width of 10 m, and a drop of 20 m. The protective coal pillar with a length of 20 m is generally reserved on both sides of the fault. However, a limestone aquifer with measured water pressure greater than 2.5 MPa about 63 m beneath the coal seam may pose a major safety challenge for underground production. The geological records have shown an urgent need to evaluate the risk of groundwater outburst around the fractured fault zone where its inrush coefficient is close to the critical value of 0.06 MPa·m⁻¹ suggested in complex structural area.

Theoretical analysis

Model establishment

The extraction of coal seam above aquifers inevitably result in stress redistribution and strata failure, and the floor strata or fault zone may be influenced by both mining and hydraulic

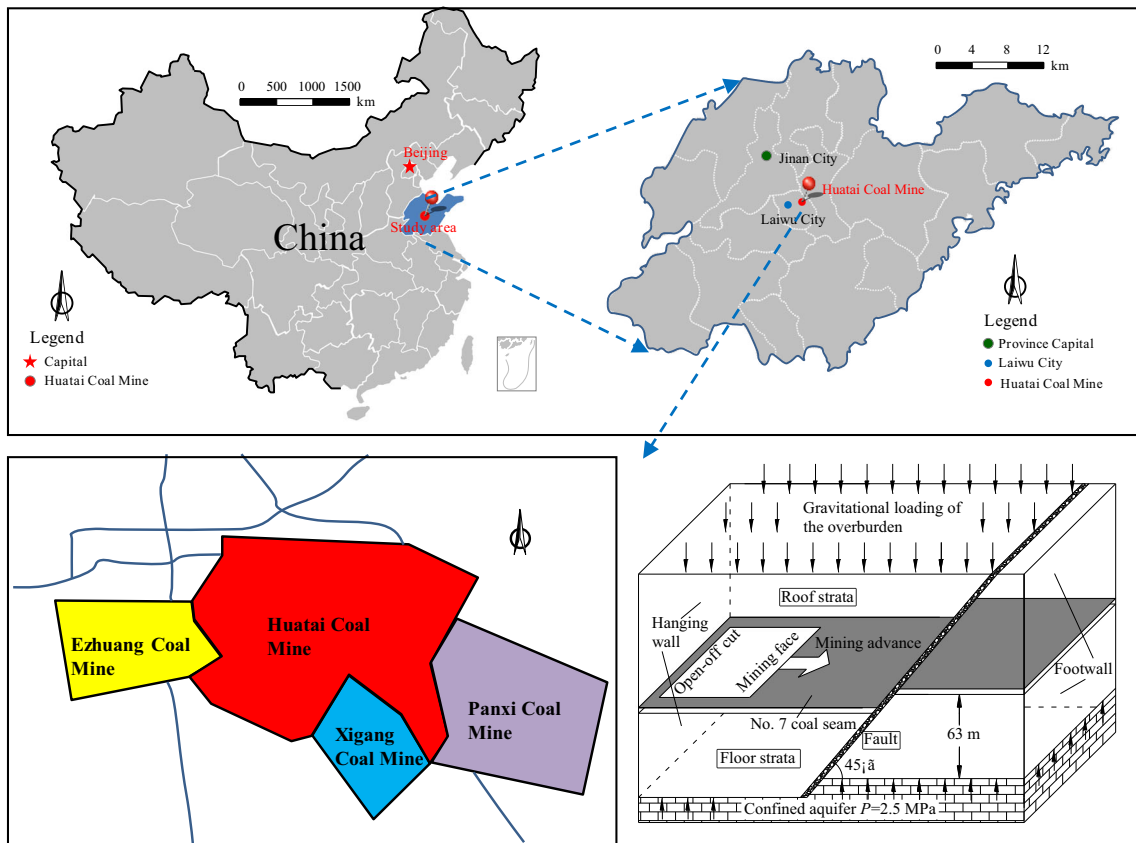
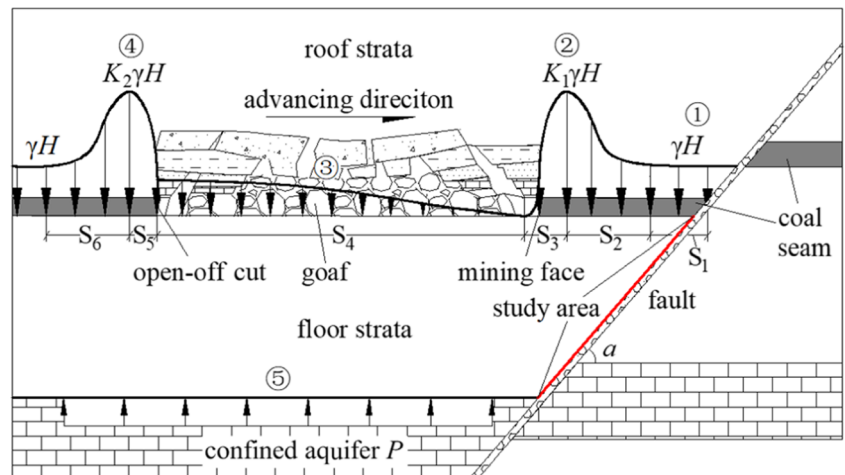


Fig. 2 Geographical location of Huatai coal mine

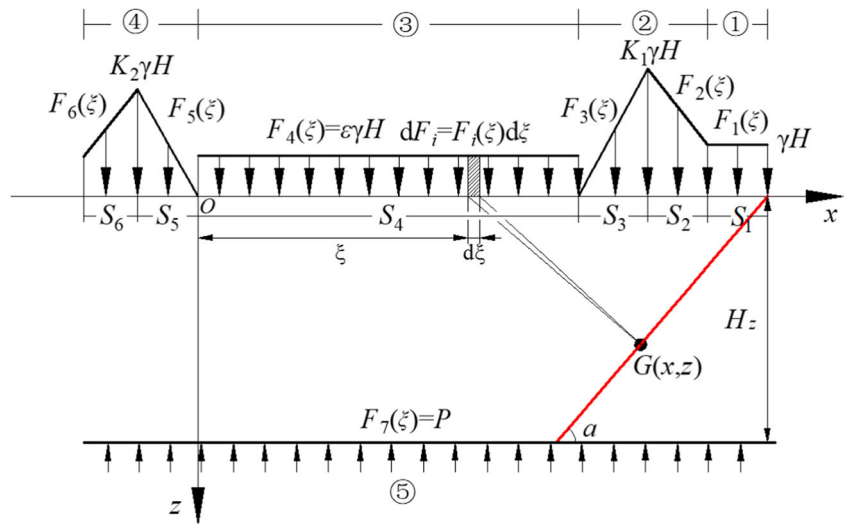
pressures (Li et al. 2011; Liu et al. 2018). Figure 3 vividly shows the external loads on the floor rock mass along the strike, in which ① indicates the undisturbed region with a stress value of γH , ② and ④ are the concentrated regions near the mining face and the open-off cut, with the stress values of $K_1\gamma h$ and $K_2\gamma H$, respectively, ③ represents the relaxed region, and the abutment pressure in this area is gradually restored owing to the compaction of roof collapsed rocks, ⑤ refers to the hydraulic region with the water pressure of P , and α is the fault dip.

Fig. 3 The external loads on the floor rock mass along the strike. ① The undisturbed region; ②, ④ the concentrated region; ③ the relaxed region; ⑤ the hydraulic region



Accordingly, the mechanical model of the fault floor shown in Fig. 4 is based on the theory elastic mechanics, which conforms to the basic assumptions of continuity and elasticity. The equivalent loads of linear distribution are adopted in the model to simplify calculations, and the load on the floor right beneath the goaf can be regarded as uniformly distributed, and its value is ϵ times of the primary rock stress. Groundwater pressure in the underlying confined aquifer, as another mechanical source on the bottom of the floor, results in an increased risk of strata failure.

Fig. 4 The mechanical model of the fault floor



The detailed expressions of all loads in Fig. 4 are listed as Eq. (1):

$$\left. \begin{aligned}
 F_1(\xi) &= \gamma H & (S_2 + S_3 + S_4 \leq \xi \leq S_1 + S_2 + S_3 + S_4) \\
 F_2(\xi) &= \frac{(K_1 - 1)[(S_2 + S_3 + S_4 - \xi) + S_2] \gamma H}{S_2} & (S_3 + S_4 \leq \xi \leq S_2 + S_3 + S_4) \\
 F_3(\xi) &= \frac{(\xi - S_4) K_1 \gamma H}{S_3} & (S_4 \leq \xi \leq S_3 + S_4) \\
 F_4(\xi) &= \varepsilon \gamma H & (0 \leq \xi \leq S_4) \\
 F_5(\xi) &= \frac{-K_2 \xi \gamma H}{S_5} & (-S_5 \leq \xi \leq 0) \\
 F_6(\xi) &= \frac{(K_2 - 1)[(S_5 + S_6 + \xi) + S_6] \gamma H}{S_6} & (-S_5 - S_6 \leq \xi \leq -S_5) \\
 F_7(\xi) &= P & (-S_5 - S_6 \leq \xi \leq S_1 + S_2 + S_3 + S_4)
 \end{aligned} \right\} \quad (1)$$

where γ indicates the average bulk density of floor rocks, H refers to the average mining depth of coal seam, K_1 and K_2 are supporting pressure coefficients of coal body near the mining face and the opening cut, respectively, P is the hydraulic pressure of the aquifer, ε is the compaction rate of the goaf, S_1 – S_6 are the lengths of corresponding mechanical loads, respectively, and H_z is the thickness of aquiclude.

If a microelement $d\xi$ is taken at a distance of ξ away from the coordinate origin O , the small concentrated force can be represented as $dF_i = F_i(\xi)d\xi$. Furthermore, the micro-stress components of $G(x, z)$ induced by dF_i are shown in Eq. (2) (Xu 2002).

$$\left. \begin{aligned}
 d\sigma_z^{(i)} &= -\frac{2F_i(\xi)d\xi}{\pi} \frac{z^3}{[z^2 + (x-\xi)^2]^2} \\
 d\sigma_x^{(i)} &= -\frac{2F_i(\xi)d\xi}{\pi} \frac{z(x-\xi)^2}{[z^2 + (x-\xi)^2]^2} \\
 d\sigma_{zx}^{(i)} &= -\frac{2F_i(\xi)d\xi}{\pi} \frac{z^3(x-\xi)}{[z^2 + (x-\xi)^2]^2}
 \end{aligned} \right\} \quad (2)$$

Equation (3) can be defined by integrating Eq. (2) from $\xi = \xi_{i1}$ to $\xi = \xi_{i2}$.

$$\left. \begin{aligned}
 \sigma_z^{(i)} &= -\frac{2}{\pi} \int_{\xi_{i1}}^{\xi_{i2}} \frac{F_i(\xi)z^3}{[z^2 + (x-\xi)^2]^2} d\xi \\
 \sigma_x^{(i)} &= -\frac{2}{\pi} \int_{\xi_{i1}}^{\xi_{i2}} \frac{F_i(\xi)z(x-\xi)^2}{[z^2 + (x-\xi)^2]^2} d\xi \\
 \tau_{zx}^{(i)} &= \int_{\xi_{i1}}^{\xi_{i2}} \frac{F_i(\xi)z^2(x-\xi)}{[z^2 + (x-\xi)^2]^2} d\xi
 \end{aligned} \right\} \quad (3)$$

Then, we can easily obtain the total stress components (σ_z , σ_x , and τ_{zx}), as shown in Eq. (4).

$$\left. \begin{aligned}
 \sigma_z &= \sum_{i=1}^7 \sigma_z^{(i)} \\
 \sigma_x &= \sum_{i=1}^7 \sigma_x^{(i)} \\
 \tau_{zx} &= \sum_{i=1}^7 \tau_{zx}^{(i)}
 \end{aligned} \right\} \quad (4)$$

where σ_z , σ_x , and τ_{zx} denote the vertical stress, horizontal stress, and shear stress, respectively.

According to the theorem of rock mechanics (Shen and Chen 2006), Eq. (5) can be used to calculate the tangential stress (τ_n) on the fault plane, as shown in Fig. 5.

$$\tau_n = \frac{\sigma_z - \sigma_x}{2} \sin 2\alpha + \tau_{zx} \cos 2\alpha \tag{5}$$

Previous studies have suggested that the process of fault activation is actually shear failure of the mining wall along the fault plane, which conforms to the mechanism triggering fault-slip tremors by induced stress changes during the excavations (Hofmann and Scheepers 2011; Ma et al. 2015; Sainoki et al. 2019). Consequently, the re-activation criterion of the geological fault within the stope floor can be exhibited as follows:

$$|\tau_n| \geq [\tau] \tag{6}$$

In Eq. (6), $[\tau]$ is the shear strength of the fault zone, which can be generally measured by laboratory tests after field sampling. When other parameters are the same, the greater the tangential stress $|\tau_n|$ is, the easier the fracture zone is to be destroyed. This will greatly promote the formation of groundwater outburst channels.

Theoretical results and discussion

This paper provides the detailed analysis of only the fault dip and mining distance due to space limitations. The configuration parameters of the mechanical model used in the current study are mainly based on the geological records and routine monitoring of the Huatai coal mine, with the following details: $\gamma = 25 \text{ kN}\cdot\text{m}^{-3}$, $S_1 = 0\text{--}170 \text{ m}$, $S_2 = S_6 = 20 \text{ m}$, $S_3 = S_5 = 10 \text{ m}$, ξ

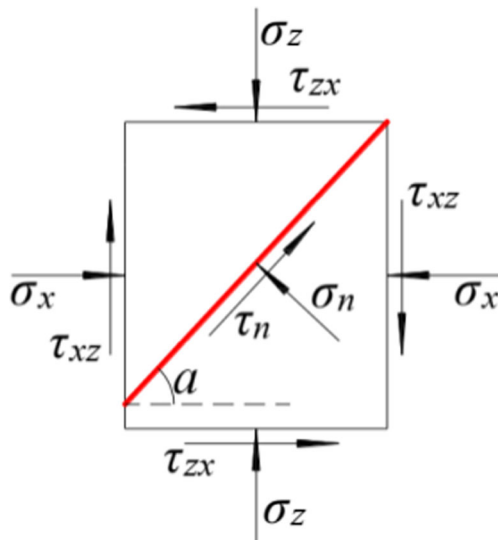


Fig. 5 Stress state of element in two-dimensional plane

$= 0.3$, $K_1 = 3.5$, $K_2 = 2.5$, $H = 650 \text{ m}$, $H_z = 70 \text{ m}$, $P = 2.5 \text{ MPa}$, $S_4 = 0\text{--}170 \text{ m}$, $\alpha = 15^\circ, 30^\circ, 45^\circ, 60^\circ, 75^\circ$.

Effect of mining distance on fault activation

Figure 6 shows the evolution of tangential stress on the fault plane with varying excavation distances. It can be seen that the geo-stress (i.e., $S_4 = 0$) in the primitive environment is approximately linear distributed. Additional shear stress may be formed owing to the excavation of coal seam, which makes the tangential stress change constantly. Moreover, the peak stress gradually approaches the coal seam floor from deep to

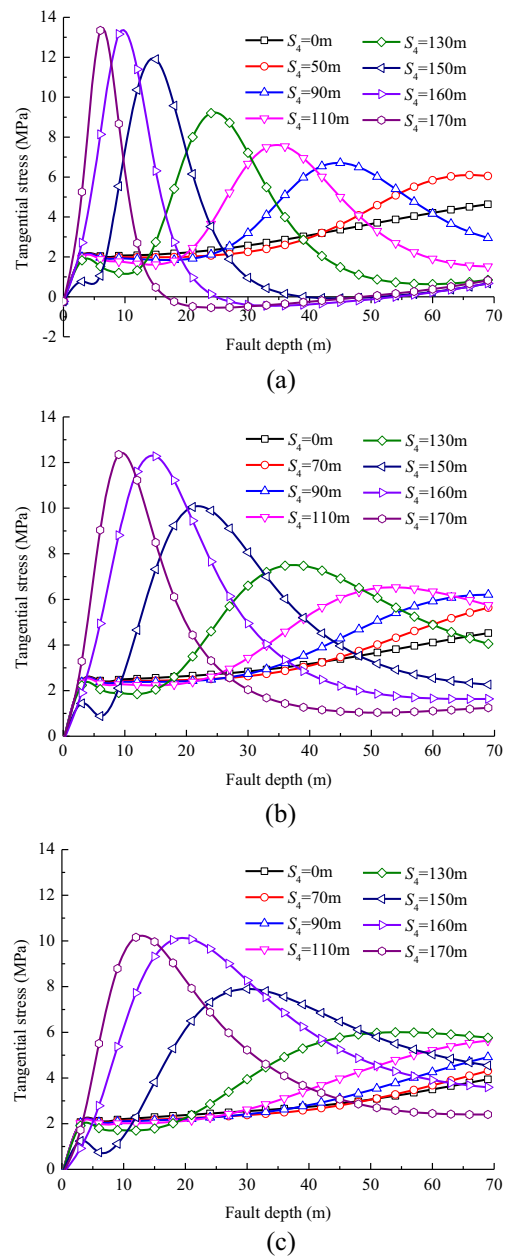


Fig. 6 Evolution of tangential stress on the fault plane with varying excavation distances. (a) 30°, (b) 45°, (c) 60°

shallow along the fault, followed by an increasing peak value. This result can provide a theoretical explanation for the frequent occurrence of groundwater outburst accidents during the mining process adjacent to faults.

Sainoki and Mitri (2014) and Jiang et al. (2020) used the safety coefficient of stress concentration (i.e., the ratio of the maximum values of post- and pre-mining stress) to evaluate the relative potential of the fault-slip and rockburst events induced by mining activities. The relation between the stress concentration factor and the mining distance is further analyzed, and the results are given in Fig. 7. There are two phases divided by the projection of the fault, i.e., phase I and phase II. The starting and ending positions with red dotted lines indicating the horizontal range of the fault projection onto the coal seam floor are $x^{(30^\circ)} = 67.19$ m, 190 m, $x^{(45^\circ)} = 120.34$ m, 190 m, and $x^{(60^\circ)} = 149.01$ m, 190 m, respectively. The calculation results of all the models (cases) present a similar trend, where the concentration factor of tangential stress in the fault zones is positively correlated with the advancing distance of the working face. Clearly, the growth rate of stress concentration at different stages is not the same. It can be seen from the comparison of Fig. 6(a) and Fig. 7(a) that the peak tangential stress in the first phase (i.e., 0–67.19 m) is relatively unchanged and located at the bottom of the fault (Fig. 6(a)). As the working face enters into the projection range (i.e., 67.19–190 m), the growth rate of stress concentrating factor increases significantly, and then remains basically constant towards the end of the second phase, following the trend of the peak stress moving from 69 m to 5 m along the fault depth. This is generally consistent with the results of the direct shear test by Meng et al. (2018), who characterize the activation process of the joint into three stages: a slowly increasing stage, a rapidly increasing stage and a nearly constant stage. Hence, for the cases with a constant fault dip, the longer the mining distance, the easier the fault re-activation will be.

Effect of fault dip angle on fault activation

The evolution of tangential stress on the fault plane with varying dips is depicted in Fig. 8. The distribution of tangential stress presents a “multi-peak” state of alternating between positive and negative. Compared with the mechanism of fault activation caused by the mining distance, the effect of fault dip is mainly manifested as the advance of the peak stress in the small-angle fault, which is reinforced by the variation of stress concentration coefficients in Fig. 7. For example, when the dip angle is 15° , the stress at different parts ranges from 0 to 14 MPa (8–17 m), -2.1 to 0 MPa (17–44 m), and 0 to 3.3 MPa (44–69 m), respectively. This exactly shows good agreement with the results of previous study on the existence of a positive to negative paired shear zones forming the damage boundary in the floor strata after excavation (Liang et al. 2020). With the increase of fault dip, the tangential stress not only decreases in

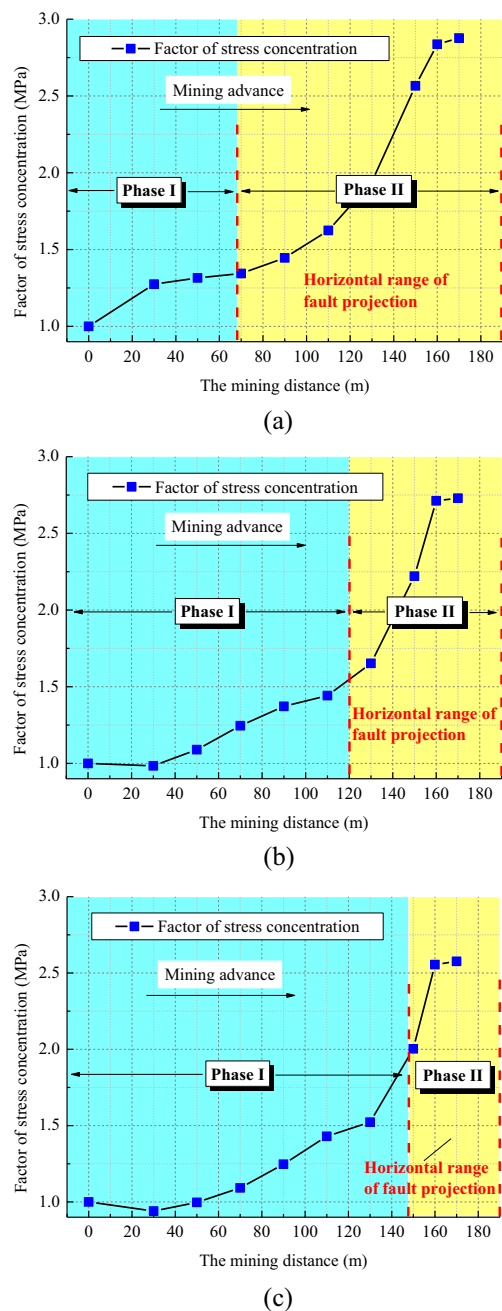


Fig. 7 Relation between the factor of stress concentration and the mining distance. (The red dotted lines represent the starting and ending positions of the fault projection onto the coal seam floor, respectively.) (a) 30° , (b) 45° , (c) 60°

peak value ($\tau_n^{(15^\circ)} = 11.4$ MPa $>$ $\tau_n^{(30^\circ)} = 9.2$ MPa $>$ $\tau_n^{(45^\circ)} = 7.5$ MPa $>$ $\tau_n^{(60^\circ)} = 6.0$ MPa $>$ $\tau_n^{(75^\circ)} = 4.6$ MPa) but also lags behind in peak position (12 m (15°), 24 m (30°), 36 m (45°), 54 m (60°), 69 m (75°)). Therefore, for the cases with a constant advancing distance, the smaller the fault dip, the earlier the fault activation distance will be. The obtained result theoretically explains why water-inrush phenomena in engineering practice are more likely to occur near the fault zone with small dips.

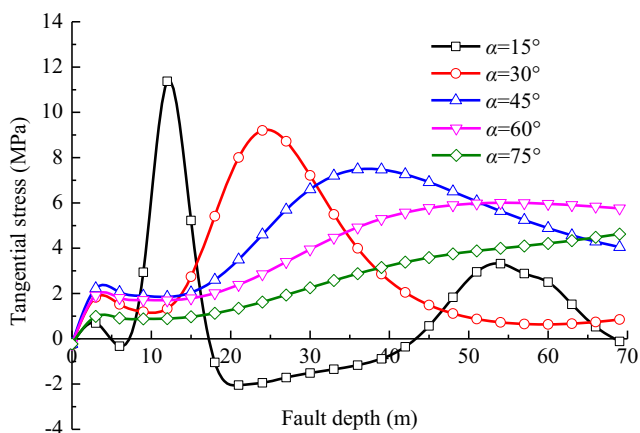


Fig. 8 Evolution of tangential stress on the fault plane with varying fault dips (cases of $S_4 = 130$ m)

Numerical simulation

Affected by mining activities, the fault state between the hanging wall and footwall may change from “adhesion” to “disconnection,” thus providing conditions for the fault to become the main inflow channel. For more detailed observations of the floor failure characteristics under hydromechanical

conditions, the numerical simulation of coal mining above aquifers was conducted by using the Fast Lagrangian Analysis of Continua (Itasca Consulting Group, Inc. 2005, version 3.0). This method has been widely employed in failure analysis problems related to geological or rock engineering (Jiang et al. 2020; Sainoki and Mitri 2014, 2016; Sainoki et al. 2019; Wu et al. 2004).

Model setup

According to the geological conditions of the Huatai coal mine, three case studies with fault dips of 30° , 45° , and 60° are implemented for coal mining above the confined aquifer. Figure 9 clearly shows the mesh division and boundary conditions for numerical models. These models include the equivalent roof and floor strata, the coal seam, the fault zone, and the confined aquifer and have the geometric dimensions of 360m (X) \times 230m (Y) \times 150 m (Z). The bottom boundary of the model is fully fixed, and an equivalent vertical load of 16.25 MPa is uniformly applied on the top boundary to represent the geo-stress induced by all overburden layers, while the horizontal displacement of the other boundaries is constrained. An initial hydraulic pressure of 2.5 MPa is set in the confined

Fig. 9 (a, b) Mesh division and boundary conditions for numerical models (a case of fault dip = 45°)

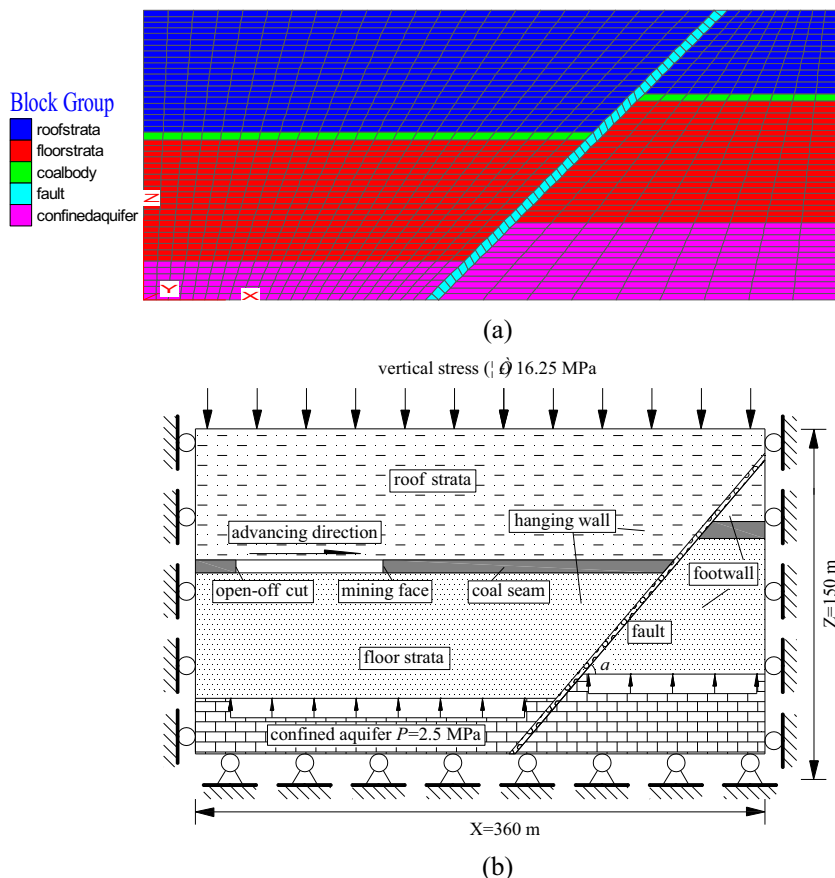


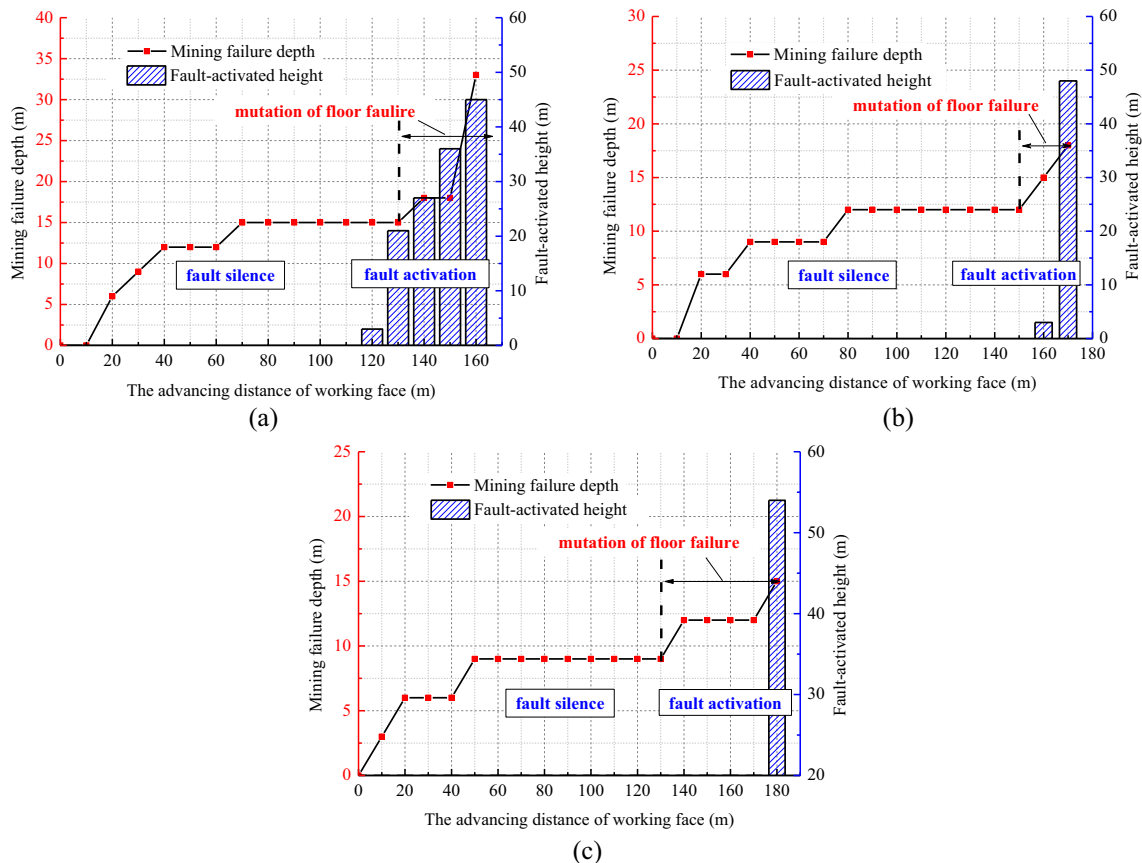
Table 1 Physico-mechanical parameters for rocks and the coal seam

Lithology	Density/ ($\text{kN}\cdot\text{m}^{-3}$)	Bulk modulus/ GPa	Shear modulus/ GPa	Cohesion/ MPa	Friction angle/ ($^{\circ}$)	Tensile strength/ MPa	Permeability/ ($\text{m}^2\cdot(\text{Pa}\cdot\text{s})^{-1}$)	Porosity
Roof strata	25.0	5.0	3.2	4.0	32	3.0	6×10^{-15}	0.3
Coal seam	13.9	2.3	2.0	2.1	20	1.1	3×10^{-13}	0.4
Floor strata	25.0	6.0	4.1	5.0	33	2.8	7×10^{-15}	0.2
Fault zone	21.0	1.0	1.25	0.1	28	0.2	5×10^{-12}	0.5
Confined aquifer	24.0	4.0	2.3	2.0	31	2.1	4×10^{-10}	0.7

aquifer to simulate the effect of groundwater on the fault floor during coal extraction. The coal seam is incrementally excavated from $X=40$ m until the critical pathway for groundwater outburst is determined. The continuum models were analyzed by hydromechanical coupling to characterize the damage and flow in the fault floor during coal mining. All failure calculations were performed according to the Mohr–Coulomb criterion. As shown in Table 1, the values of the physico-mechanical parameters for rocks and the coal seam were empirically selected according to the results of field test and research findings (Li et al. 2011; Cheng et al. 2019; Liu et al. 2020).

Numerical results and analysis

Generally, mining excavation and fault are affected mutually. When the excavation is close to the fault, the stress redistribution induced by mining and hydraulic pressures will result in fault activation, whereas the influence of fault zone on mining activities is mainly reflected in the damage range of coal seam and floor rock mass in front of the working face. Figure 10 shows the relationships between the mining failure depth, fault-activated height, and the advancing distance of working face. According to previous literature (Li et al. 2011), the mining failure depth and the fault-activated height in this

**Fig. 10** Relationships between the mining failure depth, fault-activated height, and the advancing distance of working face. (a) 30°, (b) 45°, (c) 60°

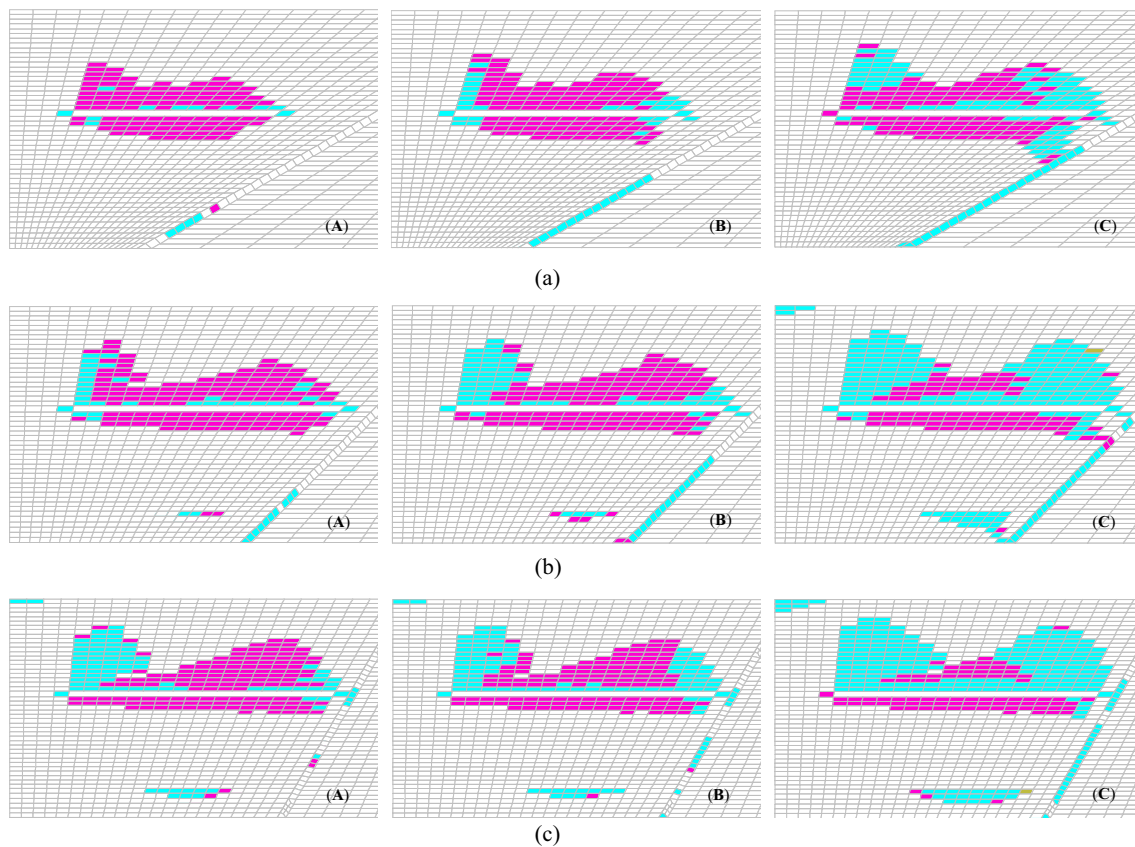


Fig. 11 Typical results of the process of fault activation. (A) the local activation stage; (B) the extension stage; (C) the transfixion stage. (a) 30°, (b) 45°, (c) 60°

study can be defined as the vertical range of failure zones in “intact” floor strata and the fault, respectively. The numerically obtained result demonstrates that the failure depth of floor increases gradually with the excavation of coal seam. For faults, it can be divided into two parts: fault silence and fault activation. Compared with the results of Fig. 6, it can be concluded that the energy storage is predominant during the fault silence period, while the damage effect is more evident during the fault activation period. Furthermore, the activation process of faults with dip angles of 30°, 45°, and 60° basically falls into the middle and late stages of mining, accompanied by a mutation of floor failure depth.

Figure 11 shows the typical results of the process of fault activation, which can be summarized as the local activation stage (A), the extension stage (B), and the transfixion stage (C). The element colors of the numerical profiles represent the damage status in the current step. It should be noted that the damage occurs in the middle and lower part of fault and then gradually expands upward with the excavation of coal seam. The simulation results exhibit good agreement with the tangential stress evolution derived in the theoretical model. Meanwhile, the damage in the mining-induced failure zone expands towards the fault re-activation zone. Gradually, the re-activation of faults becomes more active and newly

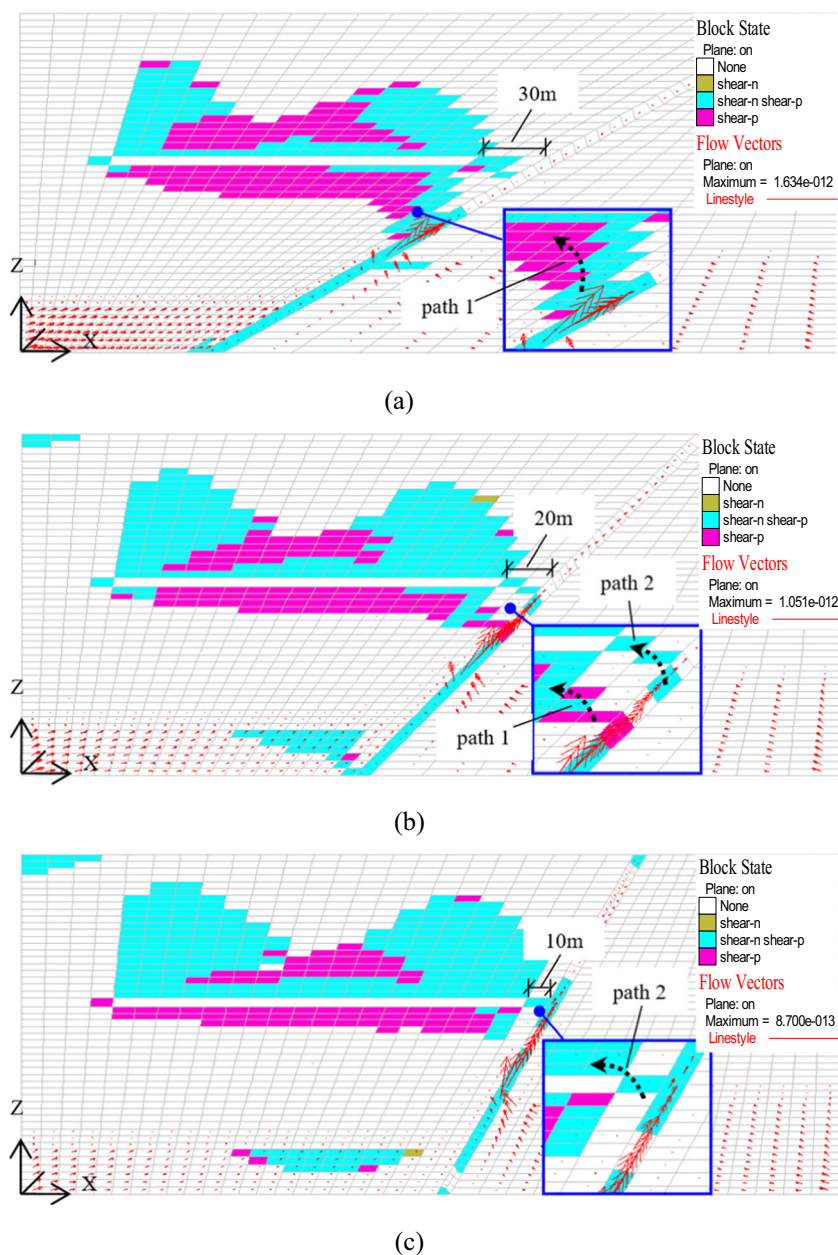
generated damage continuously develops, connects with each other until a critical pathway for groundwater outburst is formed.

Figure 12 shows the distribution of groundwater outburst pathway and seepage after all calculations. Obviously, there are two types of water-inrush channels, both of which are formed along faults. The confined water with red arrows indicating the seepage vector, as evident in Fig. 12(a), ascends progressively and bursts into the excavations through the maximum failure zone in the shallow floor strata right beneath the mining face (i.e., path 1), resulting in disastrous consequences. Owing to the increasing inclination of fault, the failure area continues to develop upward until path 2 is formed in front of the working face (Fig. 12(b) and (c)). In addition, the lengths of the critical safety pillar are roughly 30 m (30°), 20 m (45°), and 10 m (60°), respectively. The above results clearly indicate that normal faults with small dips are more prone to water inrush at the same advancing distance.

Conclusion and discussion

Mining operations above aquifers face risks of groundwater outburst through fractured floor strata. To better understand

Fig. 12 Groundwater outburst pathway and seepage distribution. (The arrows in red denote the seepage flow. The longer the arrow is, the higher the flow velocity will be. The black arrows indicate the formed or underlying inrush pathways.) **a** 30°, **b** 45°, **c** 60°



the mechanism of fault water inrush, we theoretically and numerically investigate the influence of the advancing distance and fault dip on the processes of fault activation driven by mining pressure and hydraulic pressure. The main conclusions of this study can be summarized as follows:

1. The theoretical and simulated results reveal that the process of fault activation induced by stress change is positively correlated with the advancing distance of working face, while negatively correlated with the fault dip. The peak value of tangential stress increases significantly and approaches the coal seam floor from deep to shallow along the fault during the excavation process entering into the horizontal range of fault projection, which
2. corresponds to the simulated damage extension without considering the strength reduction. Compared with the activation mechanism caused by mining distance, the effect of small-dip fault is mainly manifested as the advance of multi-peak stress of alternating between positive and negative.
2. The comparison of theoretical calculation and numerical simulation indicates the energy storage effect and the damage effect are predominant in the fault silence period and the fault activation period respectively. The whole process of fault activation can be roughly divided into three stages: the local activation stage, the extension stage, and the transfixion stage. For the cases with a constant advancing distance, the smaller the fault dip is, the earlier

the water-inrush channel will be formed. The length of critical protective pillar of the 7502 working face in Huatai coal mine is suggested to be reserved 30 m at least.

- The research results derived by the mechanical model reveals the theoretical mechanism of triggering fault activation and groundwater outburst, which is helpful for scientific understanding of the frequent occurrence of water-related hazards when the mining activities are close to faults. There are some limitations in theoretically characterizing the actual fracturing process of the fault zones with tectonic stress in underground engineering. In addition, the sensitivity analysis on rock parameters will be dealt in future studies.

Funding This study was finally supported by the National Natural Science Foundation of China (Nos. 41977219, 51779031) and the Open Fund of State Key Laboratory of Coal Resources and Safe Mining of China (No. SKLCSRSMI9KFA02).

Declarations

Conflict of interest The authors declare no competing interests.

Disclaimer The research content has no conflict of interest with the mine, and the data can be used for conducting the scientific research in “Huatai Coal Mine.”

References

- Bai HB, Ma D, Chen ZQ (2013) Mechanical behavior of groundwater seepage in karst collapse pillars. *Eng Geol* 164:101–106. <https://doi.org/10.1016/j.enggeo.2013.07.003>
- Bu WK, Xu H (2020) Research on the effect of dip angle on shear stress on normal fault plane and water inrush in floor strata during mining activities. *Geotech Geol Eng* 38:4407–4421. <https://doi.org/10.1007/s10706-020-01282-w>
- Bukowski P (2011) Water hazard assessment in active shafts in upper Silesian coal basin mines. *Mine Water Environ* 30:302–311. <https://doi.org/10.1007/s10230-011-0148-2>
- Cheng GW, Li LC, Zhu WC, Yang TH, Tang CA, Zheng Y, Wang Y (2019) Microseismic investigation of mining-induced brittle fault activation in a Chinese coal mine. *Int J Rock Mech Min Sci* 123:104096. <https://doi.org/10.1016/j.ijrmm.2019.104096>
- Donnelly LJ (2006) A review of coal mining induced fault reactivation in Great Britain. *Q J Eng Geol Hydrogeol* 39:5–50. <https://doi.org/10.1144/1470-9236/05-015>
- Gudmundsson A, Berg SS, Lyslo KB (2001) Skurtveit E (2001) Fracture networks and fluid transport in active fault zones. *J Struct Geol* 23:343–353. [https://doi.org/10.1016/S0191-8141\(00\)00100-0](https://doi.org/10.1016/S0191-8141(00)00100-0)
- Hofmann GF, Scheepers LJ (2011) Simulating fault slip areas of mining induced seismic tremors using static boundary element numerical modelling. *Min Technol* 120(1):53–64. <https://doi.org/10.1179/037178411X12942393517291>
- Hu XY, Wang LG, Lu YL (2014) Yu M (2014) Analysis of insidious fault activation and water inrush from the mining floor. *Int J Min Sci Technol* 24:477–483. <https://doi.org/10.1016/j.ijmst.2014.05.010>
- Hu Y, Sun J, Liu WQ, Wei DY (2019) The evolution and prevention of water inrush due to fault activation at working face no. ii 632 in the Hengyuan coal mine. *Mine Water Environ* 38:93–103. <https://doi.org/10.1007/s10230-018-00579-w>
- Huang Z, Jiang ZQ, Qian ZW, Cao DT (2014) Analytical and experimental study of water seepage propagation behavior in the fault. *Acta Geodyn Geomater* 11(4):361–370. <https://doi.org/10.13168/AGG.2014.0017>
- Islam MR, Shinjo R (2009) Mining-induced fault reactivation associated with the main conveyor belt roadway and safety of the Barapukuria Coal Mine in Bangladesh: constraints from BEM simulations. *Int J Coal Geol* 79:115–130. <https://doi.org/10.1016/j.coal.2009.06.007>
- Itasca Consulting Group, Inc. (2005) Fast Lagrangian Analysis of Continua in 3 dimensions, version 3.0, user’s manual. Itasca Consulting Group, Inc.
- Jiang LS, Kong P, Zhang PS, Shu JM, Wang QB, Chen LJ, Wu QL (2020) Dynamic analysis of the rock burst potential of a longwall panel intersecting with a fault. *Rock Mech Rock Eng* 53:1737–1754. <https://doi.org/10.1007/s00603-019-02004-2>
- Lamoreaux JW, Wu Q, Wanfang Z (2014) New development in theory and practice in mine water control in China. *Carbonates Evaporites* 29(2):141–145. <https://doi.org/10.1007/s13146-014-0204-7>
- Li G, Zhou W (2006) Impact of karst water on coal mining in North China. *Environ Geol* 49(3):449–457. <https://doi.org/10.1007/s00254-005-0102-3>
- Li LC, Yang TH, Liang ZZ, Zhu WC, Tang CA (2011) Numerical investigation of groundwater outbursts near faults in underground coal mines. *Int J Coal Geol* 85(3–4):276–288. <https://doi.org/10.1016/j.coal.2010.12.006>
- Li SC, Wu J, Xu YWM (2019) Mechanics criterion of water inrush from the coal floor under influence of fault and its engineering application. *Int J Geomech* 19(5):04019022. [https://doi.org/10.1061/\(ASCE\)GM.1943-5622.0001387](https://doi.org/10.1061/(ASCE)GM.1943-5622.0001387)
- Liang ZZ, Wu N, Li YC, Li H, Li WR (2019) Numerical study on anisotropy of the representative elementary volume of strength and deformability of jointed rock masses. *Rock Mech Rock Eng* 52:4387–4402. <https://doi.org/10.1007/s00603-019-01859-9>
- Liang ZZ, Song WC, Liu WT (2020) Theoretical models for simulating the failure range and stability of inclined floor strata induced by mining and hydraulic pressure. *Int J Rock Mech Min Sci* 132:104382. <https://doi.org/10.1016/j.ijrmm.2020.104382>
- Liu HL, Li LC, Li ZC, Yu GF (2018) Numerical modelling of mining-induced inrushes from subjacent water conducting karst collapse columns in northern China. *Mine Water Environ* 37:652–662. <https://doi.org/10.1007/s10230-017-0503-z>
- Liu YB, Yang HZ, Liu C (2020) Study on the influence of coal face advancing distance on fault-activated water inrush. *Geotech Geol Eng*. <https://doi.org/10.1007/s10706-020-01234-4>
- Lu YL, Wang LG (2015) Numerical simulation of mining-induced fracture evolution and water flow in coal seam floor above a confined aquifer. *Comput Geotech* 67:157–171. <https://doi.org/10.1016/j.compgeo.2015.03.007>
- Ma D, Bai HB, Wang YM (2015) Mechanical behavior of a coal seam penetrated by a karst collapse pillar: mining-induced groundwater inrush risk. *Nat Hazards* 75:2137–2151. <https://doi.org/10.1007/s11069-014-1416-9>
- Meng FZ, Zhou H, Wang ZQ, Zhang CQ, Li SJ, Zhang LM (2018) Characteristics of asperity damage and its influence on the shear behavior of granite joints. *Rock Mech Rock Eng* 51(2):429–449. <https://doi.org/10.1007/s00603-017-1315-y>
- Sainoki A, Mitri HS (2018) Quantitative analysis with plastic strain indicators to estimate damage induced by fault-slip. *J Rock Mech Geotech* 10:1–10. <https://doi.org/10.1016/j.jrmge.2017.06.001>
- Sainoki A, Mitri HS (2014) Dynamic behaviour of mining-induced fault slip. *Int J Rock Mech Min Sci* 66(1):19–29. <https://doi.org/10.1016/j.ijrmm.2013.12.003>

- Sainoki A, Mitri HS (2016) Influence of undulating fault surface properties on its seismic waves during fault-slip. *Int J Min Reclam Environ* 30(1):1–12. <https://doi.org/10.1080/17480930.2013.876808>
- Sainoki A, Mitri HS, Chinnasane D, Schwartzkopff AK (2019) Quantitative energy-based evaluation of the intensity of mining-induced seismic activity in a fractured rock mass. *Rock Mech Rock Eng* 52:4651–4667. <https://doi.org/10.1007/s00603-019-01861-1>
- Shao JL, Zhou F, Sun WB (2019) Evolution model of seepage characteristics in the process of water inrush in faults. *Geofluids* 2019:1–14. <https://doi.org/10.1155/2019/4926768>
- Shen MR, Chen JF (2006) *Mechanics of rock masses*. Tongji University Publishing House, Shanghai (in Chinese)
- Shi WH, Yang TH, Liu HL, Yang B (2018) Numerical modeling of non-Darcy flow behavior of groundwater outburst through fault using the Forchheimer equation. *J Hydrol Eng* 23(2):04017062. [https://doi.org/10.1061/\(ASCE\)HE.1943-5584.0001617](https://doi.org/10.1061/(ASCE)HE.1943-5584.0001617)
- Shi LQ, Qiu M, Wang Y, Qu XY, Liu TH (2019) Evaluation of water inrush from underlying aquifers by using a modified water-inrush coefficient model and water-inrush index model: a case study in Feicheng coalfield, China. *Hydrogeol J* 27:2105–2119. <https://doi.org/10.1007/s10040-019-01985-2>
- Sun J, Wang LG, Hu Y (2019) Mechanical criteria and sensitivity analysis of water inrush through a mining fault above confined aquifers. *Arab J Geosci* 12:4. <https://doi.org/10.1007/s12517-018-4180-4>
- Wu Q, Wang M, Wu X (2004) Investigations of groundwater bursting into coal mine seam floors from fault zones. *Int J Rock Mech Min Sci* 41(4):557–571. <https://doi.org/10.1016/j.ijrmmms.2003.01.004>
- Wu N, Liang ZZ, Li YC, Li H, Li WR, Zhang ML (2019) Stress-dependent anisotropy index of strength and deformability of jointed rock mass: insights from a numerical study. *B Eng Geol Environ* 78: 5905–5917. <https://doi.org/10.1007/s10064-019-01483-5>
- Wu Q, Hao ZC, Zhao YW, Xu H (2020) Prediction of concealed faults in front of a coalface using feature learning. *B Eng Geol Environ* 79: 4191–4204. <https://doi.org/10.1007/s10064-020-01800-3>
- Xu ZL (2002) *Concise tutorial on elasticity*. Higher Education Press, Beijing (in Chinese)
- Xu JP, Liu SD, Wang B, Zhang P, Gui H (2012) Electrical monitoring criterion for water flow in faults activated by mining. *Mine Water Environ* 31:172–178. <https://doi.org/10.1007/s10230-012-0184-6>
- Xue YG, Kong FM, Qiu DH, Su MX, Zhao Y, Zhang K (2021) The classifications of water and mud/rock inrush hazard: a review and update. *B Eng Geol Environ* 80:1907–1925. <https://doi.org/10.1007/s10064-020-02012-5>
- Yang T, Liu HY, Tang CA (2017) Scale effect in macroscopic permeability of jointed rock mass using a coupled stress–damage–flow method. *Eng Geol* 228:121–136. <https://doi.org/10.1016/j.enggeo.2017.07.009>
- Yin SX, Zhang JC, Liu DM (2015) A study of mine water inrushes by measurements of in situ stress and rock failures. *Nat Hazards* 79: 1961–1979. <https://doi.org/10.1007/s11069-015-1941-1>
- Zhang R, Jiang ZQ, Zhou HY, Yang CW, Xiao SJ (2014) Groundwater outbursts from faults above a confined aquifer in the coal mining. *Nat Hazards* 71(3):1861–1872. <https://doi.org/10.1007/s11069-013-0981-7>
- Zhang SC, Guo WJ, Li YY, Sun WB, Yin DW (2017) Experimental simulation of fault water inrush channel evolution in a coal mine floor. *Mine Water Environ* 36:443–451. <https://doi.org/10.1007/s10230-017-0433-9>
- Zhu WC, Wei CH (2011) Numerical simulation on mining-induced water inrushes related to geologic structures using a damage-based hydro-mechanical model. *Environ Earth Sci* 62(1):43–54. <https://doi.org/10.1007/s12665-010-0494-6>
- Zhu GL, Zhang WQ, Wang SL, Zhang PS (2018) Experimental research on characteristics of fault activation and confined water rising. *Geotech Geol Eng* 36:2625–2636. <https://doi.org/10.1007/s10706-018-0487-x>